Giant Rashba-type Spin Splitting in Ferroelectric GeTe(111)

Marcus Liebmann, Christian Rinaldi, Domenico Di Sante, Jens Kellner, Christian Pauly, Rui Ning Wang, Jos Emiel Boschker, Alessandro Giussani, Stefano Bertoli, Matteo Cantoni, Lorenzo Baldrati, Ivana Vobornik, Giancarlo Panaccione, Dmitry Marchenko, Jaime Sanchez-Barriga, Oliver Rader, Raffaella Calarco, Silvia Picozzi, Riccardo Bertacco, and Markus Morgenstern*

Dr. M. Liebmann, J. Kellner, Dr. Chr. Pauly, Prof. M. Morgenstern
II. Institute of Physics B and JARA-FIT
RWTH Aachen University
52074 Aachen, Germany
E-mail: mmorgens@physik.rwth-aachen.de

Dr. Chr. Rinaldi, S. Bertoli, Prof. M. Cantoni, L. Baldrati, Prof. R. Bertacco
Dipartimento di Fisica
Politecnico di Milano and IFN-CNR
Via Colombo 81
20133 Milano, Italy

Dr. D. DiSante
Consiglio Nazionale delle Ricerche CNR-SPIN
UOS L'Aquila
Via Vetoio 10
67100 L'Aquila, Italy
Department of Physical and Chemical Sciences
University of L'Aquila
Via Vetoio 10
67100 L'Aquila, Italy

R. Wang, Dr. J. E. Boschker, Dr. A. Guissani, Dr. R. Calarco
Paul-Drude-Institut für Festkörperelektronik
Hausvogteiplatz 5-7
10117 Berlin, Germany

Dr. I. Vobornik, Dr. G. Panaccione
Consiglio Nazionale delle Ricerche, CNR - IOM
Laboratorio TASC,
34149 Trieste, Italy

Dr. D. Marchenko
Physikalische und Theoretische Chemie
Freie Universität Berlin
Takustraße 3
14195 Berlin, Germany

Dr. J. Sanchez-Barriga, Prof. O. Rader
Helmholtz-Zentrum für Materialien und Energie
Elektronenspeicherring BESSY II
Albert-Einstein-Strasse 15
12489 Berlin, Germany

Prof. S. Picozzi
Consiglio Nazionale delle Ricerche CNR-SPIN
UOS L'Aquila
Via Vetoio 10
67100 L'Aquila, Italy

The Rashba effect as an electrically tunable spin-splitting is anticipated to be the key for semiconductor-based spintronics.[1-4] It has been pursued in semiconductor heterostructures,[5-7] where advanced experiments found tunable spin signals at low temperature.[8-10] Recently, bulk spin splittings came back into focus[11,12] and bulk Rashba bands have been found in the layered polar semiconductors BiTeCl and BiTeI.[13-16] While these Rashba bands are not tunable by external fields, an electrically switchable bulk-Rashba system has been discovered theoretically: the room-temperature ferroelectric semiconductor GeTe (Curie temperature: ~700 K).[17] Such a material would lead to a non-volatile control of the Rashba induced spin precession and appears to be scalable, since the ferroelectricity in GeTe persists down to the nm-scale.[18,19] In addition, the large separation of the two spin branches by about 0.19 Å^{-1} [17] implies a complete rotation of spins within ~3.5 nm only[5] (Rashba parameter $\alpha \approx 5$ eV Å) pointing to a small footprint of possible spin-transistors.

However, so far, the Rashba bands of GeTe have not been probed experimentally. Here, we present spin-polarized angularly resolved photoelectron spectroscopy (ARPES) of GeTe(111) compared with density-functional theory (DFT) calculations. We identify a novel surface Rashba band with giant spin splitting as well as fingerprints of the predicted bulk Rashba band, both showing excellent agreement between DFT and ARPES. Both Rashba

bands cut the Fermi level E_F and, thus, will contribute to the spin transport of GeTe. Moreover, we experimentally confirm the relation between Rashba band helicity and non-volatile ferroelectric polarization determined by piezo force microscopy (PFM).

Single-domain epitaxial α-GeTe(111) films (thickness: 32 nm) are grown by molecular beam epitaxy (MBE) on in-situ prepared Si(111) and are transferred in ultra-high vacuum (UHV) to the apparatus allowing for high-resolution ARPES. PFM images are recorded afterwards on the same sample ex-situ.

The upper left inset in **Figure 1a** shows the noncentrosymmetric structure (space group R3m) of ferroelectric GeTe with displaced adjacent Ge and Te layers along [111] providing a net dielectric polarization.[20] The DFT calculations reveal that the depicted upwards polarization P_{up} is by 30 meV/formula unit more favorable than the downwards polarization P_{dn} in accordance with earlier calculations.[21] The layered displacement provides the inversion symmetry breaking which, by spin-orbit coupling, leads to the Rashba spin splitting of the bulk bands.[17] Figure 1b and c show the calculated band structures of P_{up} and P_{dn} for the Te- terminated surface after a rigid downwards shift of E_F by 200 meV (see below). The band structures exhibit spin-split hole-type surface states partly energetically overlapping with the bulk Rashba band. The number of surface bands and their splitting are different for P_{up} and P_{dn}. For the energetically favored P_{up} configuration, the spin polarization is clockwise (counter-clockwise) for the outer (inner) surface Rashba band. Ge-terminated surfaces require a much higher formation energy by 60 meV/$Å^2$ largely independent on the Ge chemical potential[21] and show a much smaller spin splitting of the surface states in contrast to the experiment (Figure S1).

In order to determine the intrinsic polarization of GeTe, we performed PFM experiments (Figure 1a). They reveal a reproducible, ferroelectric hysteresis with ±10 %

3

variation of the coercive voltage at ~100 different spots of the surface. When sweeping the tip voltage from 0 V towards positive voltage within a virgin area (black dotted line), the phase jumps by 180° signaling that the unpoled sample polarization P_1 corresponds to P_{up}. This favorably agrees with our DFT simulations favoring P_{up}, too. The hysterisis loop, shifted towards positive tip voltage, reveals a second remanent state P_2, which allows writing of non-volatile ferroelectric domains (Figure 1a, bottom inset).

Figure 2a-b represent the bulk and surface Brillouin zone of GeTe(111) with high symmetry points marked. The known six-fold symmetric shape of the bulk Rashba band[17] is displayed on the ZAU hexagonal surface of the bulk Brillouin zone. Figure 2c-f display the ARPES band dispersion (electron energy E vs. wave vector $\underline{k}$) at photon energy hν=20 eV, i.e. close to the ZAU plane,[22] along the high symmetry directions ZA (k_x) and ZU (k_y). The bands calculated by DFT for P_{up} are overlaid in Figure 2e-f. Notably, all spectral features in the experiment correspond to bulk and surface valence bands from the calculation after the rigid downwards shift of E_F by 200 meV, which is expected from the known p-type doping of GeTe by Ge vacancies.[23] The overlap shows that bulk bands (solid lines in Figure 2e and f) and surface bands (dashed and dotted lines) are clearly discernable in some regions, e.g., the bands at highest $|k_x|$ for $E >- 0.4$ eV in Figure 2e are the surface bands S_1, S_2 and S_3, while the bands at $E < - 0.2$ eV and $|k_y| < 0.2$ Å^{-1} correspond to the bulk bands B_1 and B_2. The measured $|k_x|$ distance between the two surface Rashba bands $\Delta|k_x| = 0.14$ Å^{-1} perfectly agrees with the DFT calculations for P_{up}, whereas it is $\Delta|k_x| = 0.24$ Å^{-1} in the DFT calculation for P_{dn}. This and the absence of a second pair of surface Rashba bands in the ARPES data (not shown) corroborates again that P_{up} is the energetically favorable state in the as grown sample.

The region at $|\underline{k}| < 0.2$ Å^{-1} and $E \in [-0.2\,\text{eV}, 0.0\,\text{eV}]$ is crowded with DFT bands imply-ing possible superpositions of bulk and surface states. For example, S_1, S_2 and B_1 could contribute to the upwards moving bands close to $k_x = 0.0$ Å^{-1} and S_3 and B_1 could be responsi-

ble for the same band moving downwards at higher $|k_x|$ (Figure 2e). Constant energy maps are used to disentangle the states further. Figure 2g-h show such maps at E_F close to the ZAU plane overlaid with marks deduced from DFT for the surface states S_1 and S_2 (g) and the bulk state B_1 (h) in the high symmetry directions. One observes that S_1 and S_2 exhibit stars with tips along k_y ($\overline{\Gamma M}$), while B_1 shows stars with tips along k_x (ZA) in, both, ARPES and DFT data. The triangles connecting the inner and the outer star (see arrow) are instead most likely related to S_3.[22] We do not observe any indications of surface band bending,[22,25] such that the picture emerging from ARPES largely reflects the bulk band line-up with respect to E_F within the bulk as relevant for future deployment of GeTe in spintronic devices. Notably, both, bulk and surface Rashba bands cross E_F.

In order to corroborate the bulk and surface nature of the bands, we performed a hν dependent mapping of the band structure (**Figure 3** and S2-S4).[22] Thereby, we probe the $\underline{k}$ dependence of the bands along k_z, i.e. perpendicular to the ZAU surface. The outer stars attributed to S_1 and S_2 as well as the arms connecting the inner and outer star attributed to S_3 do not disperse with k_z. In contrast, the inner circle (Figure 3a-c) and the inner bands (Figure 3d-f) exhibit dispersion, such that they are related to bulk bands. Most likely, they belong to a hybridization of B_1 and S_3. Indeed, plotting the states from the DFT slab calculation with their intensity in separate surface layers (not shown) points to a considerable hybridization between B_1 and S_3 at the surface.

Figure 3g-i show the (k_x,k_y)-maps at higher binding energy, where B_1 and B_2 are well separated from surface states (see Figure 2). The bulk bands from DFT are overlaid. Note that they develop from a six-fold to a three-fold symmetry away from ZAU. Experimentally, a concave intensity line appears along the minimal positions of the DFT lines (arrows in g) and some intensity at the double arms running along k_x. Since the bulk bands do not disperse down to -0.5 eV along k_x (ZA), the bright feature at the corners of the figures belong to S_2 as

identified by dispersion plots. Thus, also isolated features of the bulk Rashba band are identified, but their weak intensity, their intrinsic broadening, and their small k splitting (0.03 Å^{-1}) makes it challenging to disentangle B_1 from B_2 and to probe their spin polarization.

The larger splitting of S_1 and S_2 allows determining their spin polarization straightforwardly (**Figure 4**). The four arrows i-iv sketched in the inset show the resultimg in-plane spin directions at four $\underline{k}$-points deduced from the spin signals obtained in two perpendicular directions parallel to the surface.[22] The main image displays the corresponding spin polarization, which clearly appears in the energy region of the surface states close to E_F exhibiting a lower value for the inner bands (iii and iv) probably related to the stronger overlap of S_2 with other bands. The spin directions (inset) are largely perpendicular to $\underline{k}_\parallel$ as expected. Notably, the spin direction of the outer (inner) surface band is clock-wise (counter-clockwise) in accordance with the DFT calculations for P_{up}. To corroborate this result further, we crosschecked the relative spin orientation between DFT and ARPES using $Sb_2Te_3(0001)$ data recorded by the same apparatus.[26] Thus, a consistent relation between spin helicity found by spin-polarized ARPES and the preferential ferroelectric polarization deduced concurrently from DFT, ARPES and PFM data is established. This implies that nonvolatile ferroelectricity guides the helicity of Rashba bands.

In summary, spin-polarized ARPES data of GeTe(111) reveal a surface Rashba band with giant k splitting of 0.14 Å^{-1}, as well as signatures of the recently predicted bulk Rashba band. Both Rashba bands cross the Fermi level and, thus, are expected to dominate the transport properties of GeTe. A connection between the energetically favorable ferroelectric polarization direction (outwards) and the spin polarization of the surface state is established, showing for the first time that ferroelectricity is directly connected to the Rashba effect. The observed coexistence of a Rashba-type surface state and a spin-polarized helical bulk state at E_F, principally switchable in spin direction with the direction of ferroelectric polarization, points to fascinating novel opportunities for spin-dependent transport.

Note added in proof: During the preparation of the manuscript, we became aware of similar results posted to arXiv.[27]

Experimental Section

Preparation of GeTe film, UHV transfer and sample properties: GeTe samples are epitaxially grown by MBE on $2 \times 2 cm^2$ sized Si(111) substrates (p-type B-doped, resistivity 1– 10 Ωcm, miscut < 0.1°, 100 nm thermal oxide capping layer).[28] The substrates are suitably wet-cleaned before loading them into the MBE system. Annealing at 150°C in the load-lock (pressure $p < 10^{-7}$mbar) and subsequent annealing at 350°C in the transfer chamber ($p < 10^{-8}$ mbar) ensure desorption of residual water from the surface before introducing the substrate into the growth chamber ($p \approx 2 \cdot 10^{-10}$ mbar). The substrates are properly treated to obtain a Si(111)-($\sqrt{3} \times \sqrt{3}$))R30°-Sb surface[29] before cooling down to the deposition temperature at 255°C. The deposition is performed using Ge and Te dual-filament effusion cells set at $T_{Ge\text{-}base}=1120°$ / $T_{Ge\text{-}tip}=1140°C$ and $T_{Te\text{-}base}=332.5$ / $T_{Te\text{-}tip}=465.5°C$. The deposition time was 90 minutes leading to 32 nm thick α-GeTe films. The sample holder fits, both, into the MBE and into the ARPES chamber such that samples are transferred in-situ using a vacuum shuttle with $p < 10^{-9}$ mbar. Hall bars of identically prepared samples revealed p-type conductivity with a bulk carrier density of 2.2×10^{26} m^{-3}. The film quality after the ARPES measurements was cross-checked by low energy electron diffraction revealing the expected hexagonal symmetry and x-ray photoelectron spectroscopy showing Ge and Te related peaks only, without any indications of chemical shifts.

Angular resolved photoelectron spectroscopy (ARPES): ARPES and spin-polarized ARPES spectra were measured in UHV at 300 K with electron analyzers Scienta R8000 and SPECS PHOIBOS 150, respectively, using linearly polarized synchrotron radiation from the beamlines UE112-PGM-1 and UE112-lowE-PGM2 at BESSY II. Spin resolution is achieved

with a Rice University Mott polarimeter operated at 26 kV (Sherman function $S_{\mathrm{eff}} = 0.16$) and capable of recording the two orthogonal spin directions in the surface plane of the sample. The energy and momentum resolution without (with) spin analysis are 20 meV (100 meV) and 0.007 Å^{-1} (0.05 Å^{-1}), respectively. We use variable hν to probe the $\underline{k}$ space perpendicular to the (111) surface.

Piezo force microscopy (PFM): Piezo force microscopy (PFM) was performed by a Keysight 5600LS atomic force microscope operating in single-frequency excitation mode using Veeco Instruments Inc. tips (SCM-PIC, Antimony (n) doped Si, L= 450 µm, k= 0.2 N/m) with a Cr(3 nm)/PtIr5(20 nm) conductive coating. The driving amplitudes were 1-2 V$_{ac}$ and the driving frequencies were 20 or 70 kHz. The piezoresponse signal has been calibrated scanning a periodically-poled lithium niobate reference sample. In order to avoid possible artifacts from electrostatic effects, we verified that the ferroelectric response does not depend on the DC voltage applied to the sample (excluding the influence of Maxwell stress). [30] The vertical and lateral response of the cantilever was monitored simultaneously probing out-of-plane and in-plane ferroelectric polarization, respectively. Only out-of-plane oriented ferroelectric domains were found.

DFT calculations: The bulk Rashba bands were calculated in the distorted rhombohedral setting.[17] For surface Rashba bands, instead, the hexagonal setting was used, due to the intrinsic hexagonal symmetry of the α-GeTe(111) or α-GeTe(0001) surface. Supercell calculations were performed using the generalized gradient approximation as implemented in the Vienna Ab-Initio Simulation Package (VASP).[31,32] We used the projector augmented wave method by explicitly treating 4 and 6 valence electrons, respectively, for Ge (4s2 4p2) and Te (5s2 5p4), while d electrons were kept within the core of the PBE pseudopotentials. Integration over the first Brillouin zone was made with a 8×8×1 Monkhorst-Pack k-mesh centered at Γ. For all simulations, a 400 eV plane-wave energy cutoff was used and a criterion

WILEY-VCH

of, at least, 0.1 meV per atom was placed on the self-consistent convergence of the total energy. Partial occupancies of wavefunctions were set according to the second order Methfessel-Paxton method with a 0.2 eV-large smearing. Spin-orbit coupling has been self-consistently taken into account. Dipole corrections, as implemented in VASP, were applied along the z direction in order to counteract any spurious electric field that might arise from periodic boundary conditions in the presence of a dipole moment normal to the surface. We considered a slab containing 7 hexagonal unit cells of α-GeTe stacked along the [0001] direction, with an additional Te layer to simulate two Te-terminated surfaces (43 atoms in the supercell) and a 20 Å-thick layer of vacuum. The atomic starting positions are chosen according to the bulk calculation.[17] Before relaxation, the two surfaces are, hence, inequivalent representing P_{up} at one surface and P_{dn} at the other surface. After atomic relaxation, both surfaces exhibit P_{up},[21] which causes a disappearance of the forces between adajacent unit cells and a layer of β-GeTe in the center of the slab. In order to mimic, both, P_{up} and P_{dn} , the band structure of the unrelaxed surface was used. Surface states correspond to states with a weight of more than 0.05 per Te surface atom.

Supporting Information
Supporting Information is available from the Wiley Online Library or from the author.

[1]   S. A. Wolf, D. D. Awschalom, R. A. Buhrmann, J. M. Daughton, S. von Molnar, M. L. Roukes, A. Y. Chtelkanova, D. M. Treger, *Science* **2001**, 294, 1488.

[2]   I. Zutic, J. Fabian, S. Das Sarma, *Rev. Mod. Phys.* **2004**, 76, 323.

[3]   S. Maekawa (ed.), *Concepts in Spin Electronics*, Oxford University Press, Oxford, UK **2006**.

[4]   D. D. Awschalom, M. E. Flatte, *Nature Phys.* **2007**, 3, 153.

[5]   S. Datta, B. Das, *Appl. Phys. Lett.* **1990**, 56, 665.

[6]   J. Nitta, T. Akazaki, H. Takayanagi, T. Enoki, *Phys. Rev. Lett.* **1997**, 78, 1335.

[7]   G. Engels, J. Lange, T. Schäpers, H. Lüth, *Phys. Rev. B* **1997**, 55, 1958.

[8]   H. C. Koo, J. H. Kwon, J. Eom, J. Chang, S. H. Han, M. Johnson *Science* **2009**, 325, 1515.

[9]   J. Wunderlich, B. G. Park, A. C. Irvine, L. P. Zârbo, E. Rozkotová, P. Nemec, V. Novák, J. Sinova, T. Jungwirth, *Science* **2010**, 330, 1801.

[10]   C. Betthausen, T. Dollinger, H. Saarikoski, V. Kolkovsky, G. Karczewski, T. Wojtowicz, K. Richter, D. Weiss, *Science* **2012**, 337, 324.

[11]   X. Zhang, Q. Liu, J. W. Luo, A. J. Freeman, A. Zunger, *Nature Phys.* **2014,** 10, 387.

[12]   G. Dresselhaus, *Phys. Rev.* **1955**, 100, 580.

[13] K. Ishizaka, M. S. Bahramy, H. Murakawa, M. Sakano, T. Shimojima, T. Sonobe, K. Koizumi, S. Shin, H. Miyahara,　　A. Kimura, K. Miyamoto, T. Okuda, H. Namatame, M. Taniguchi, R. Arita, N. Nagaosa, K. Kobayashi, Y. Murakami, R. Kumai, Y. Kaneko, Y. Onose, Y. Tokura, *Nature Mater.* **2011**, 10, 521.

[14] J. S. Lee, G. A. H. Schober, M. S. Bahramy, H. Murakawa, Y. Onose, R. Arita, N. Nagaosa, Y. Tokura, *Phys. Rev. Lett.* **2011**, 107, 117401.

[15] C.-R.Wang, J.-C. Tung, R. Sankar, C.-T. Hsieh, Y.-Y. Chien, G. Y. Guo, F. C. Chou, W.-L. Lee, *Phys. Rev. B* **2013**, 88, 081104.

[16] M. Sakano, M. S. Bahramy, A. Katayama, T. Shimojima, H. Murakawa, Y. Kaneko, W. Malaeb, S. Shin, K. Ono, S. Kumigashira, R. Arita, N. Nagaosa, H. Y. Hwang, Y. Tokura, K. Ishizaka, *Phys. Rev. Lett.* **2013**, 110, 107204.

[17] D. Di Sante, P. Barone, R. Bertacco, S. Picozzi, *Adv. Mat.* **2013**, 25, 509.

[18] M. J. Polking, M.-G. Han, A. Yourdkhani, V. Petkov, C. F. Kisielowski, V. V. Volkov, Y. Zhu, G. Caruntu, A. P. Alivisatos, R. Ramesh, *Nature Mater.* **2012***, 11, 700.

[19] A. V. Kolobov, D. J. Kim, A. Giussani, P. Fons, J. Tominaga, R. Calarco, A. Gruverman, *Appl. Phys.Lett. Mat.* **2014**, 2, 066101.

[20] T. Chattopadhyayt, J. X. Boucherlet, H. G. von Schnering, *J. Phys. C: Solid State Phys.* **1987**, 20, 1431.

[21] V. L. Deringer, M. Lumeij, R. Dronskowski, *J. Phys. Chem. C* **2012**, 116, 15801.

[22] See supporting information.

[23] M. Wuttig, D. Lüsebrink, D. Wamwangi, W. Welnic, M. Gilleszen, R. Dronskowski, *Nature Mater.* **2007**, 6, 122.

[24] P. Zhang, P. Richard, T. Qian, Y. M. Xu, X. Dai, H. Ding, *Rev. Sci. Instr.* **2011**, 82, 043712

[25] L. Kronik, Y. Shapira, *Surf. Sci. Rep.* **1999**, 37, 1.

[26] C. Pauly, G. Bihlmayer, M. Liebmann, M. Grob, A. Georgi, D. Subramaniam, M. R. Scholz, J. Sanchez-Barriga, A. Varykhalov, S. Blügel, O. Rader, M. Morgenstern, *Phys. Rev. B* **2012**, 86, 235106.

[27] J. Krempaský, H. Volfová, S. Muff, N. Pilet, G. Landolt, M. Radović, M. Shi, D. Kriegner, V. Holý, J. Braun, H. Ebert, F. Bisti, V.A. Rogalev, V.N. Strocov, G. Springholz, J. Minár, J. H. Dil, arXiv:1503.05004.

[28] R.-N. Wang, J. Boschker, E. Bruyer, D. Di Sante, S. Picozzi, K. Perumal, A. Giussani, H. Riechert, R. Calarco, *J. Phys. Chem C* **2014***,* 118, 29724.

[29] J. E. Boschker, J. Momand, V. Bragaglia, R.-N. Wang, K. Perumal, A. Giussani, B. J. Kooi, H. Riechert, R. Calarco, *Nano Lett.* **2014**, 14, 3524.

[30]   M. Alexe, A. Gruverman, *Nanoscale Characterization of Ferroelectric Materials. Scanning Probe Microscopy Approach*, Springer-Verlag, Berlin Heidelberg New York **2004**.

[31] G. Kresse, J. Furthmüller, *Phys. Rev. B* **1996**, 54, 11169.

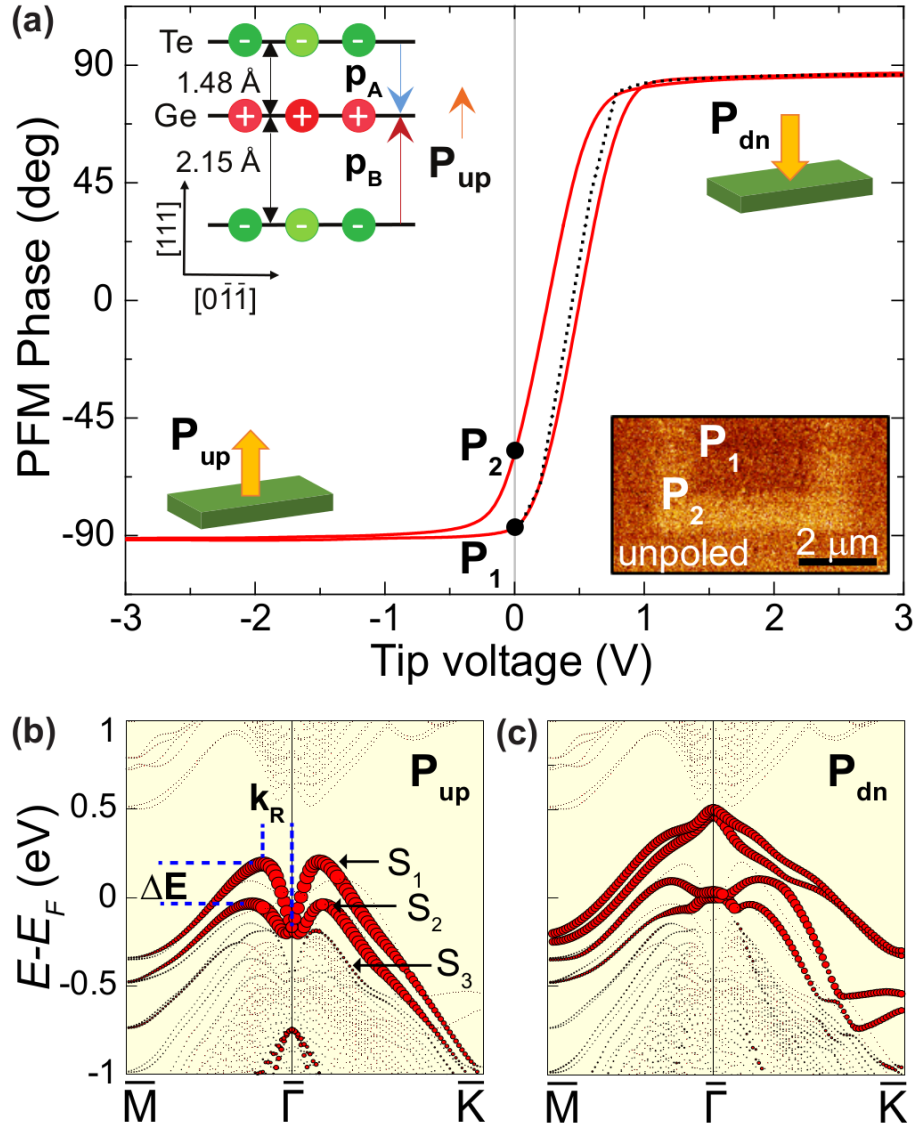[32] G. Kresse, D. Joubert, *Phys. Rev. B* **1999**, 59, 1758.

Figure 1. (a) PFM phase signal with tip voltage scanned from $V= 0$ V to $V= 3$ V (dotted line) and in a loop from $V = 3$ V via $V= -3$ V to $V= 3$ V (solid line). P_1, P_2 mark the two remanent states of polarization. Polarization directions are sketched at saturation. Upper left inset: sketch of ferroelectric GeTe along [111] with polarization P_{up} marked. Lower right inset: PFM image recorded at $V= 0$ V after writing, firstly, a P_2 domain at $V= 5$ V and, secondly, a smaller P_1 domain at $V=-5$ V into the P_2 domain. (b), (c) Band structure of GeTe slab using the atomic positions from the relaxed GeTe bulk calculation. The diameter of the red circles marks the weight of the state within the surface Te layer; small black dots correspond to bulk states. Within (b), S_1-S_3 label the surface states, ΔE marks the energy separation of the surface Rashba bands and k_R the distance of the maximum to Γ. $\overline{\Gamma K} = 0.99$ Å^{-1}, $\overline{\Gamma M} = 0.86$ Å^{-1}.
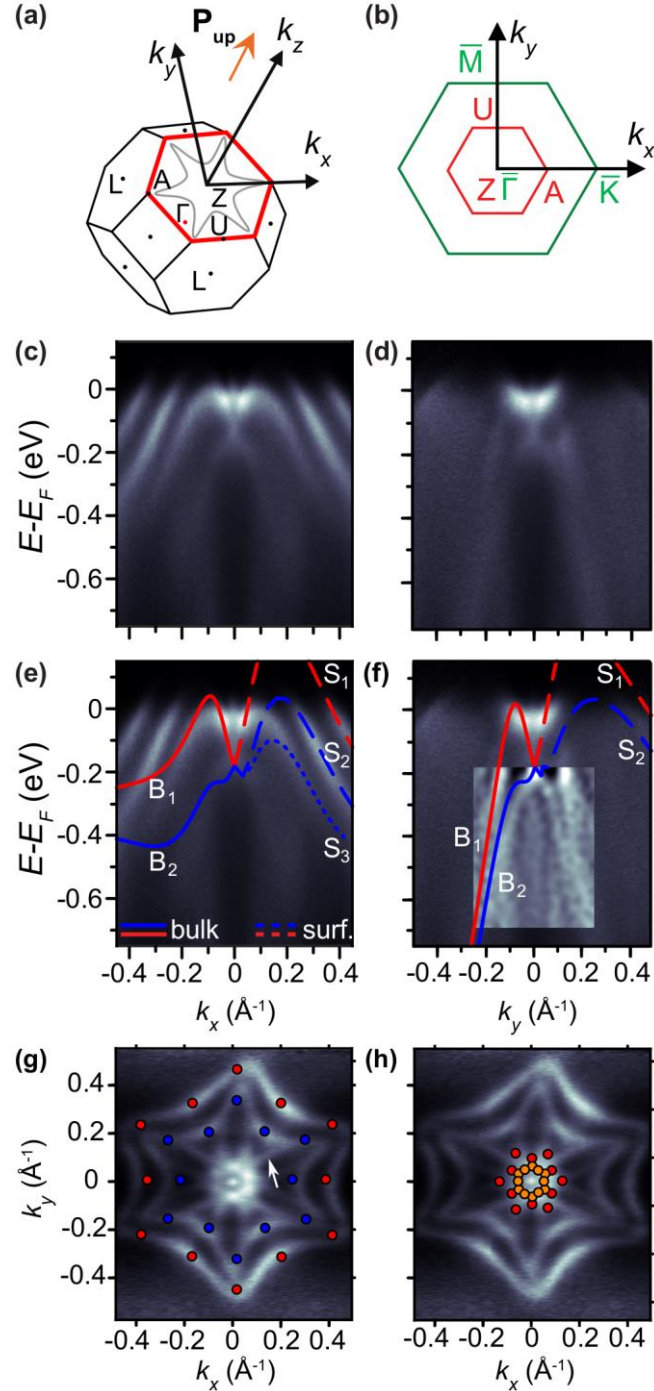
Figure 2: (a) Brillouin zone of GeTe with high symmetry points marked and ZAU surface encircled in red. The grey six-fold star indicates the constant energy map for the bulk Rashba band close to E_F. (b) Surface Brillouin zone (green hexagon) and projection of the hexagonal face of the bulk Brillouin zone (red hexagon) with synonymous ZU (ZA), $\overline{\Gamma M}$ ($\overline{\Gamma K}$) and k_x (k_y) directions marked. (c) ARPES data along $\overline{\Gamma K}$ (ZA) at photon energy $h\nu = 20$ eV. (d) Same as (c) along $\overline{\Gamma M}$ (ZU). (e) Same as (c) with overlaid bulk bands (full lines labeled B_i) from the bulk calculation and surface bands (dashed/dotted lines labeled S_i) from the slab calculation. (f) Same as (e) along $\overline{\Gamma M}$ (ZU) partly using the 2D curvature representation [24]. (g), (h) Photoelectron intensity distribution in the (k_x,k_y) plane at E_F and $h\nu = 20$ eV with overlaid surface states (g) and bulk states (h) (dots) along the high symmetry directions as deduced from DFT simulations. Arrow in (g) marks a feature most likely belonging to S_3 [22].
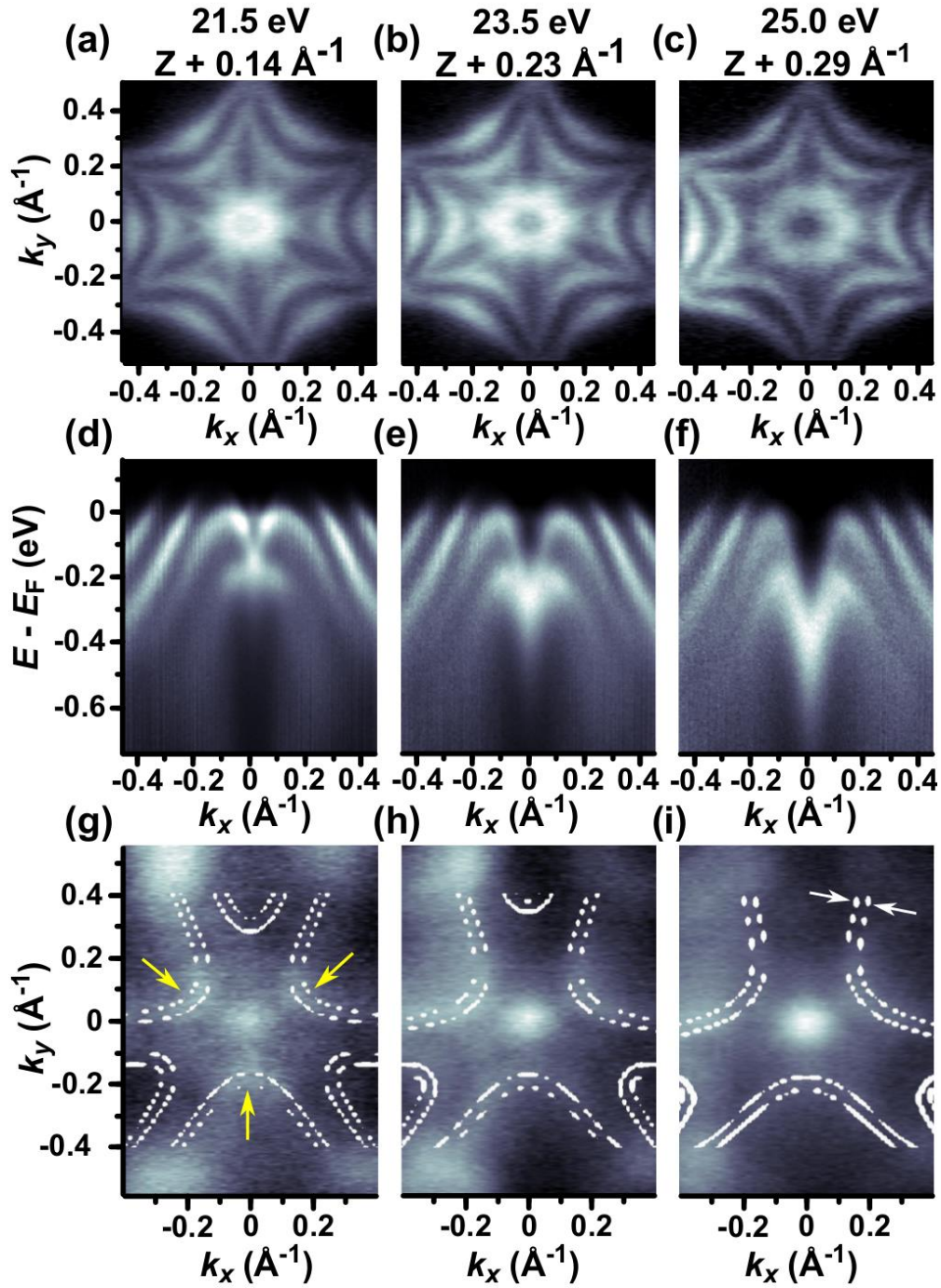
14

Figure 3: (a)-(c) Photoelectron intensity in the (k_x, k_y) plane at E_F recorded at hν as marked. The corresponding k_z values, also marked, are deduced assuming an inner potential $V_{inner} = 15$ eV after determining the Z point by the symmetry of the bands along k_z [22]. (d)-(f) Photoelectron intensity in $E(k_\parallel)$ representation along k_x (ZA, $\overline{\Gamma}\overline{K}$) at h$\nu$ as marked above the corresponding row. (g)-(i) same as (a)-(c) at a binding energy of 0.5 eV with the calculated bulk bands B_1 and B_2 overlaid. Arrows in (g) mark features described within the text. Arrows in (i) mark the $|\Delta\underline{k}|$-splitting of 0.03 Å^{-1}.
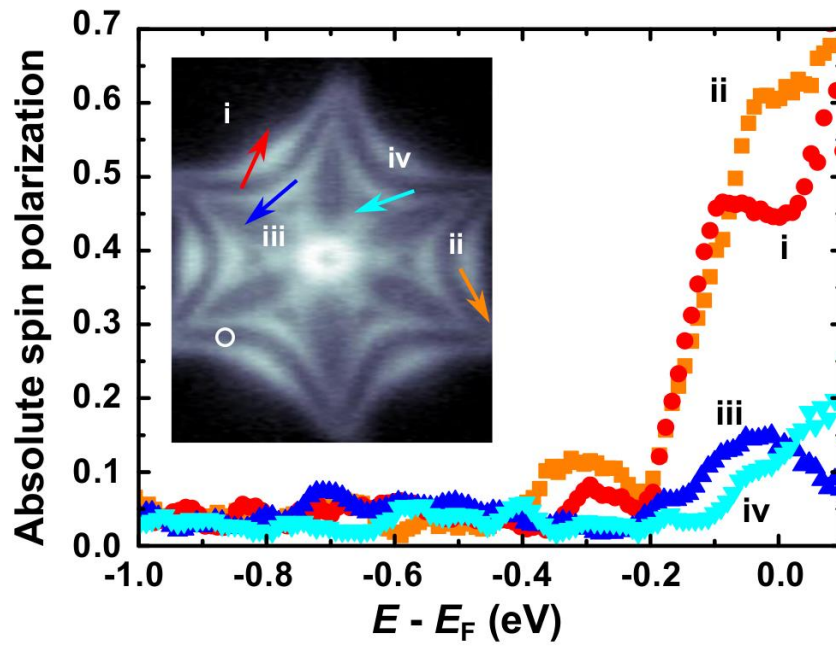
Figure 4: Spin polarization determined by spin polarized ARPES [22] at hν= 22.5 eV and the $\underline{k}_\parallel$ values marked by arrows in the inset ((k_x,k_y) map at E_F and hν= 22.5 eV). The direction of the arrows mark the spin directions determined at E_F -0.05 eV. The finite angular resolution of the experiment is sketched as a circle with full width at half maximum of the resolution function in the lower left corner.

The table of contents entry should be 50−60 words long

Photoelectron spectroscopy in combination with piezoforce microscopy reveals that the helicity of Rashba bands is coupled to the non-volatile ferroelectric polarization of GeTe(111). A novel surface Rashba band is found and fingerprints of a bulk Rashba band are identified by comparison with density functional theory calculations.

Rashba band helicity coupled to ferroelectric polarization

Marcus Liebmann, Christian Rinaldi, Domenico Di Sante, Jens Kellner, Christian Pauly, Rui Ning Wang, Jos Emiel Boschker, Alessandro Giussani, Stefano Bertoli, Matteo Cantoni, Lorenzo Baldrati, Ivana Vobornik, Giancarlo Panaccione, Dmitry Marchenko, Jaime Sanchez-Barriga, Oliver Rader, Raffaella Calarco, Silvia Picozzi, Riccardo Bertacco, and Markus Morgenstern*

Giant Rashba-type Spin Splitting in Ferroelectric GeTe(111)

ToC figure ((Please choose one size: 55 mm broad × 50 mm high **or** 110 mm broad × 20 mm high. Please do not use any other dimensions))

Supporting Information

Giant Rashba-type Spin Splitting in Ferroelectric GeTe(111)

Marcus Liebmann, Christian Rinaldi, Domenico Di Sante, Jens Kellner, Christian Pauly, Rui Ning Wang, Jos Emiel Boschker, Alessandro Giussani, Stefano Bertoli, Matteo Cantoni, Lorenzo Baldrati, Ivana Vobornik, Giancarlo Panaccione, Dmitry Marchenko, Jaime Sanchez-Barriga, Oliver Rader, Raffaella Calarco, Silvia Picozzi, Riccardo Bertacco, and Markus Morgenstern*

1. DFT calculations of Ge-terminated GeTe(111)

Figure S1a shows the calculated band structure of the Ge-terminated GeTe(111) slab sketched in Figure S1 b. Surface states are marked by red dots. The surface band within the band gap has a much weaker spin splitting of $\Delta|\underline{k}| \approx 0.02$ Å^{-1} than found for the Te-surfaces. Thus, besides the fact that Ge-terminated surfaces are energetically unfavorable by 60 meV/ Å^2, we can also rule out them by comparison with our ARPES data.
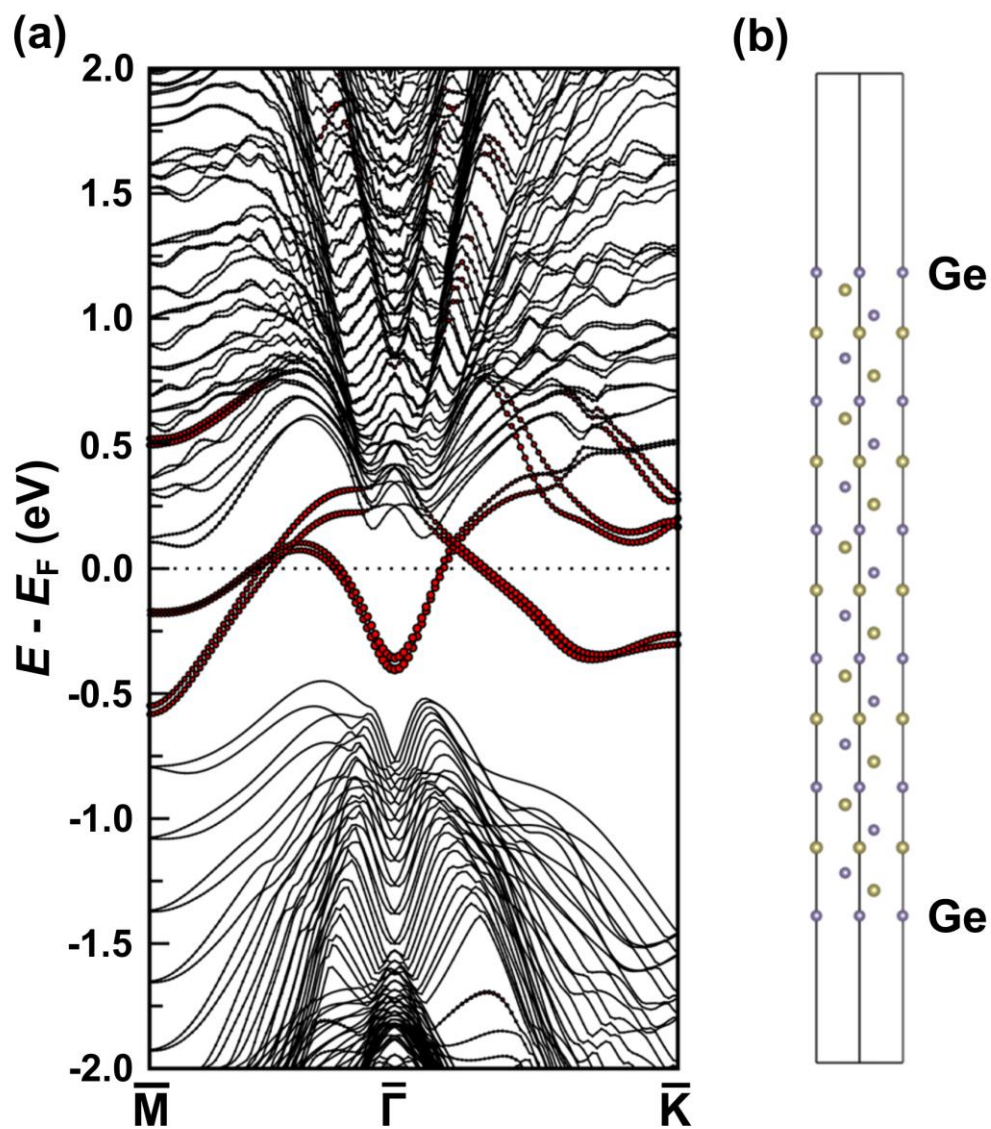
(a)

(b)

Figure S1: (a) Band structure of GeTe slab using the atomic positions from the relaxed GeTe bulk calculation with a Ge surface layer. The diameter of the red circles marks the weight of the state within the surface Ge layer; small black dots are bulk states. $\overline{\Gamma}\overline{K} = 0.99$ Å^{-1}, $\overline{\Gamma}\overline{M} = 0.86$ Å^{-1}. (b) Structural model of the calculated slab.

2. Determination of the ZAU plane

Figure S2 shows additional photoelectron intensity distributions. They are displayed within the (k_x, k_y) plane (Figure S2a) at E_F as well as an $E(k_∥)$ representation along ZA ($\overline{\Gamma}\overline{K}$) (Figure S2b) and along ZU ($\overline{\Gamma}\overline{M}$) (Figure S2c). They are partly recorded at lower hν than in Figure 3 of the main text and partly at intermediate energies as marked. The size of the inner circle obviously changes exhibiting a minimum diameter somewhere between hν = 17.5 eV and hν = 20.0 eV. The band structures in Figure S2b and c are largely symmetric around hν = 17.5 eV. Figure S2d-e show cuts through the band structure from which the diameter of the inner ring as a function of photon energy can be determined as the distance between the peak positions, which is then displayed in Figure S2f. We get a minimum diameter at hν = 18.5 ± 1 eV, which is compatible with the hv-related symmetries of all other features visible in Figure S2 and Figure 3 of the main text. Thus, we assume hν = 18.5 eV as the photon energy probing the ZAU plane and calculate the other k_z values by an inner potential of V_{inner} = 15 eV. In Figure 2 of the main text, we present data taken at 20 eV, since this photon energy allowed to record high quality spectra at a rather small deviation from the Z point (only 0.07 Å^{-1} to be compared with the extension of the Brillouin zone in the out-of-plane direction ΓZ=0.91 Å^{-1}).
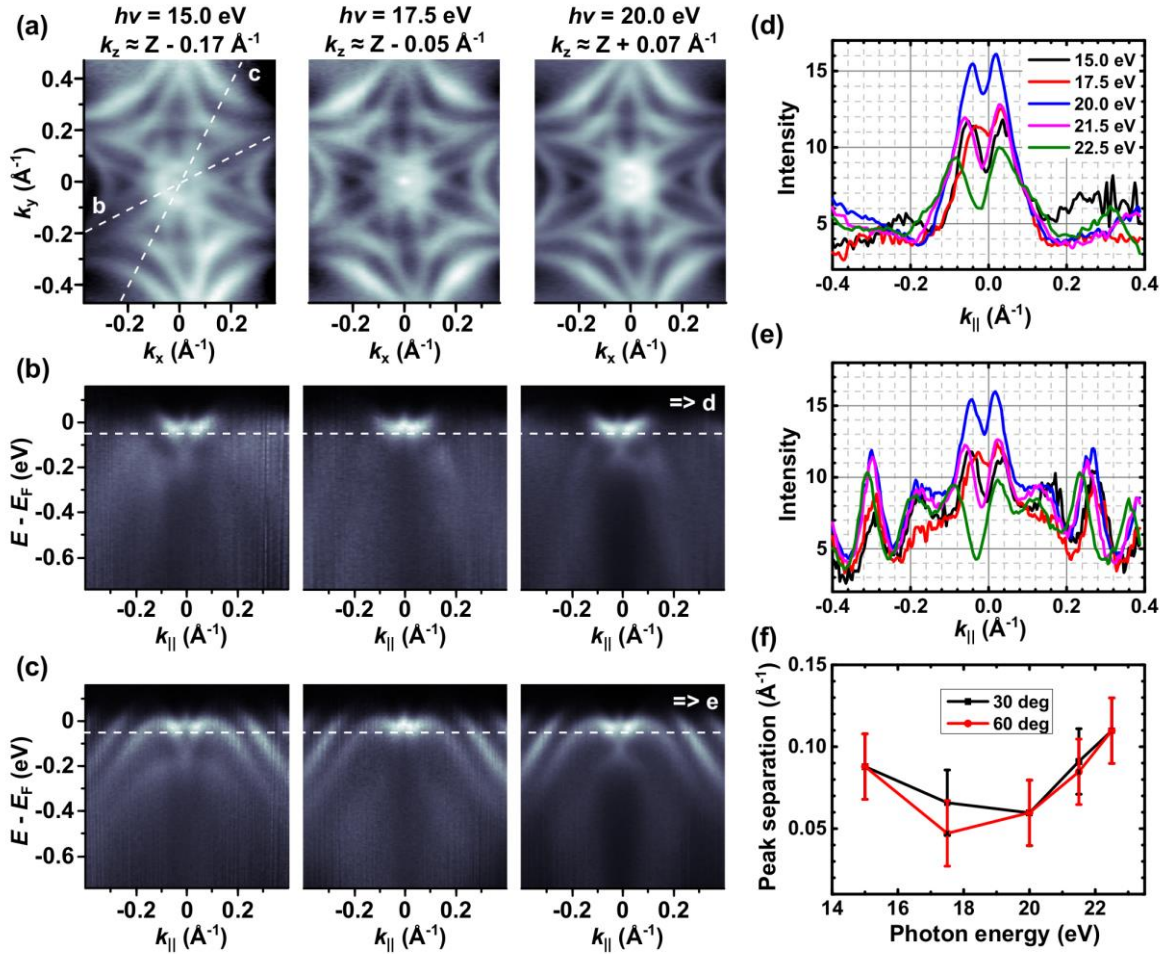
Figure S2: (a) Photoelectron intensity in the (k_x,k_y) plane at E_F and the photon energies marked. The corresponding k_z value, also marked, is deduced assuming an inner potential of $V_{inner} = 15$ eV after determining the Z point by the symmetry of the bands along k_z to be at $h\nu = 18.5$ eV. The lines marked b and c indicate the k directions of the plots in (b) and (c), respectively. (b) Photoelectron intensity in $E(k_\parallel)$ representation along ZA ($\overline{\Gamma K}$) at $h\nu$ as marked above the corresponding row. (c) Same as (b) along k_y (ZU, $\overline{\Gamma M}$). Dashed lines in (b) and (c) mark the energies used for the curves in (d) and (e), respectively. (d), (e) photoelectron intensity as a function of $k_\parallel$ along the lines drawn in (b) and (c) at the photon energies marked. (f) Diameter of the inner circle (distance between peaks in (d) (30 deg) and (e) (60 deg)) as a function of photon energy $h\nu$ (symbols). Lines are guides to the eye.

3. ARPES data at different hν along k_y

Figure S3 shows the same data as Figure 3a-f of the main text in combination with hν

dependent data along k_y (ZU, $\overline{\Gamma}\overline{M}$) in order to highlight the dispersion of the bulk bands
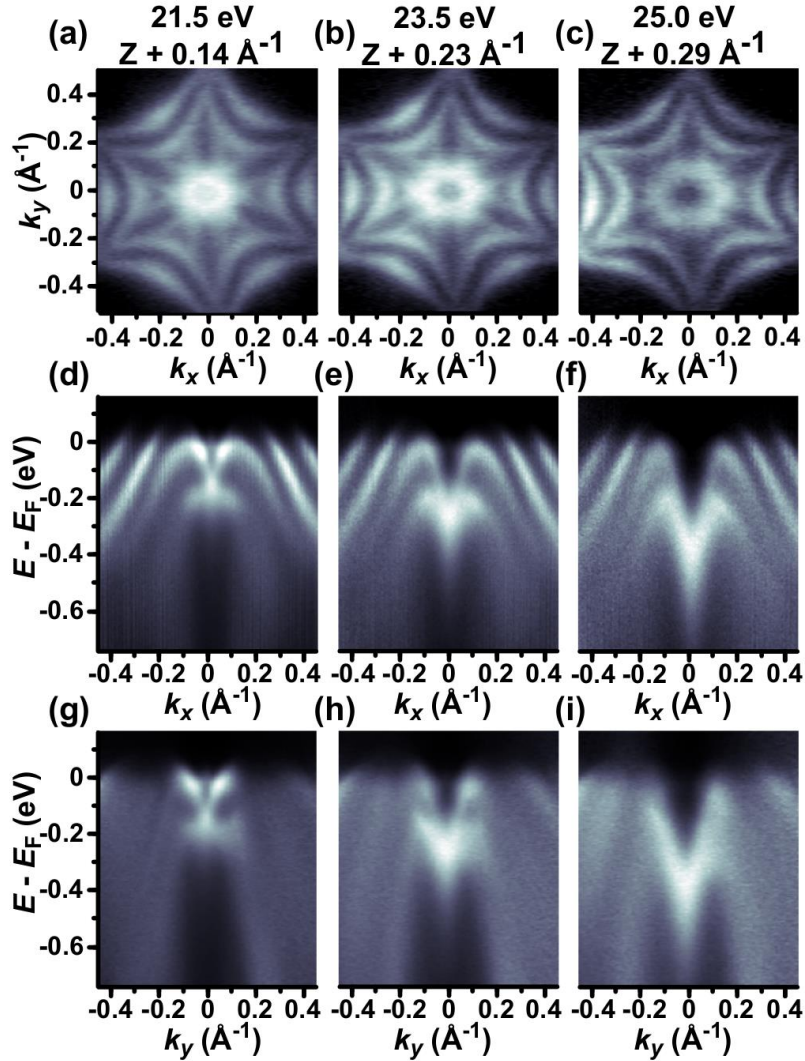
along this direction, too.

Figure S3: (a)-(c) Photoelectron intensity in the (k_x,k_y) plane at E_F recorded at hν as marked.

The corresponding k_z values, also marked, are deduced assuming an inner potential V_{inner}= 15

eV after determining the Z point by the symmetry of the bands along k_z [22]. (d)-(f)

Photoelectron intensity in $E(k_∥)$ representation along k_x (ZA, $\overline{\Gamma}\overline{K}$) at hν as marked above the

corresponding row. (g)-(i) same as (d)-(f) along k_y (ZU, $\overline{\Gamma}\overline{M}$).

4. Mapping the possible S3 state

In order to probe the origin of the arms connecting the inner structure related to B_1 and the surfaces state S_2, Figure S4b, c, e and f shows diagonal cuts through these arms as marked in Figure S4a and d at two different photon energies. The additional band exhibits a V-type structure perpendicular to the ΓK direction with an origin at -0.1 eV (Figure S4b). This structure barely disperses with k_z, albeit it appears more blurred at $h\nu = 25$ eV (Figure S4e). Figure S4b and e reveal another structure which is degenerate with S_2 at E_F, but has a stronger slope in $E(k_\parallel)$ than S_2 again without dispersion in k_z (arrows). These two features might belong to the same band representing a hole like state with Rashba splitting along k_y only and with a changing crossing point along k_x. We assume that this state is the state S3 from the DFT calculation. Indeed, it develops into the state, which has a strong overlap with the calculated S_3 state along k_x (not shown). However, due to the limited k-space resolution of the slab calculation, we currently cannot confirm the Rashba splitting in perpendicular direction.
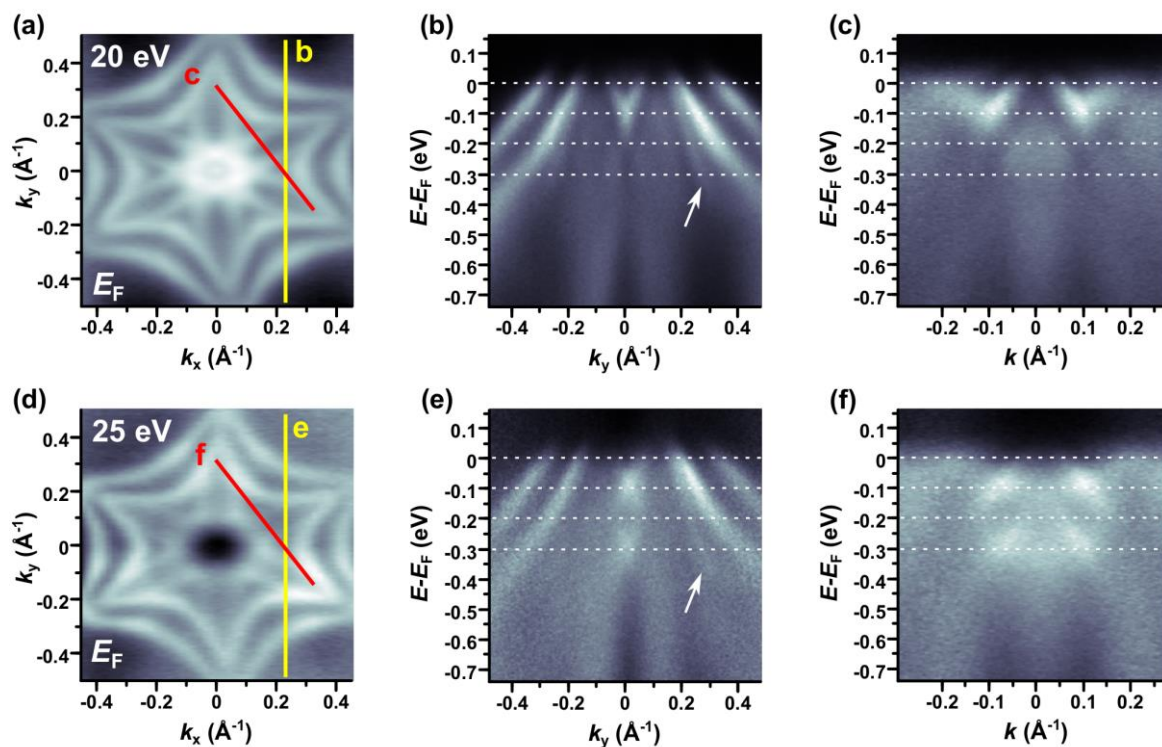
Figure S4: (a), (d) Photoelectron intensity in the (k_x, k_y) plane at E_F at the photon energies marked. The lines indicate the $\underline{k}$ space directions along which the $E(k_\parallel)$ representations in (b), (c), (e), and (f) are displayed. (b), (c), (e), (f) Photoelectron intensity in $E(k_\parallel)$ representation recorded along the $k_\parallel$ lines marked in (a) and (d). The dashed lines are drawn at the same energy in (b), (c), (e), and (f). The arrows in (b) and (e) mark a feature probably belonging to S3.

5. Surface Photovoltage

Since ARPES gives access to the band structure within a probing depth of just a few Å from the surface, while for spintronic devices bulk properties are of major relevance, we addressed the question of possible surface band bending. To this scope we determined the compensating surface photovoltage using

(A) the temperature dependence of the band structure and

(B) the energy dependence of spectral features on photoelectron intensity.

Figure S5a-b show the $E(k_\parallel)$ representation along k_y (ZU, $\overline{\Gamma}\overline{M}$) at two different temperatures. Besides the higher sharpness of the Fermi distribution at lower temperature, the band positions relative to E_F remain identical. This indicates negligible band bending towards the surface. To corroborate this finding, we also looked at the photon intensity dependence at $T = 30$ K of a singular $I(E)$ spectrum recorded at $k_\parallel = 0.0$ Å^{-1} and $h\nu = 22.5$ eV. If one increases the photon intensity by an order of magnitude (Figure S5c), we do not observe any changing peak energies with respect to E_F within 10 meV.
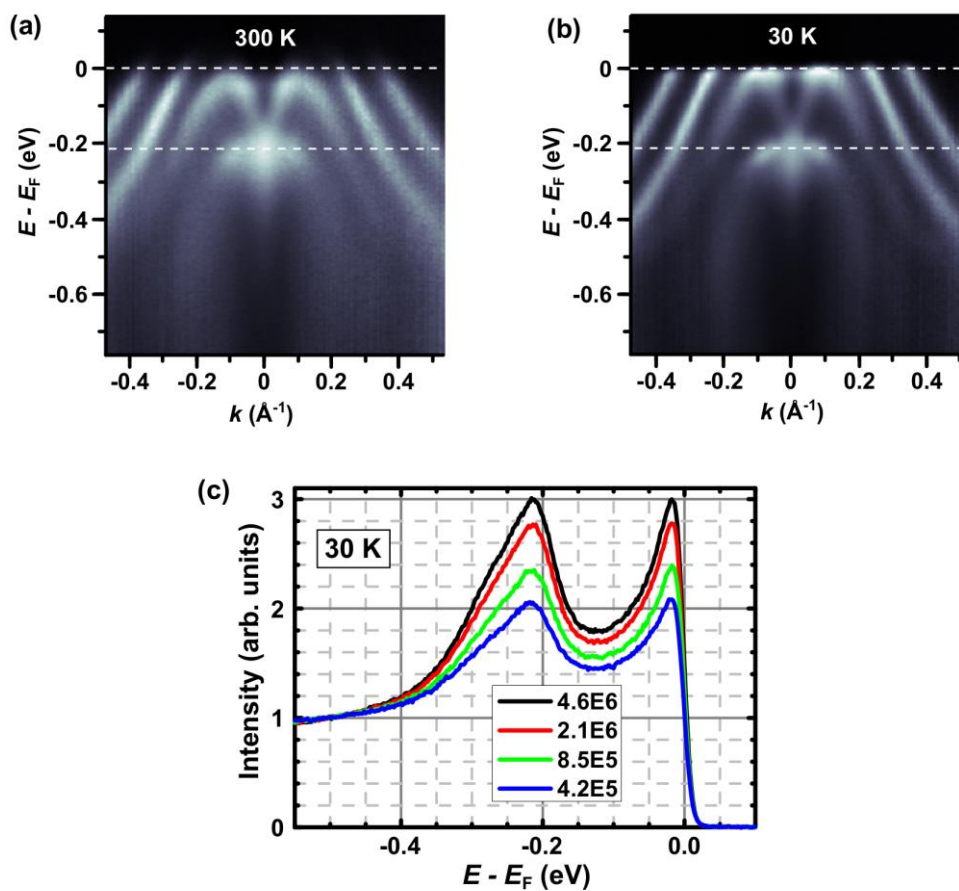
Figure S5: (a), (b) Photoelectron intensity in $E(k_\parallel)$ representations along k_x (ZA, $\overline{\Gamma}\overline{K}$)

recorded at hν = 22.5 eV and T = 300 K (a), 30 K (b). The white lines mark the same

binding energy with respect to E_F in (a) and (b). (c) Photoelectron intensity as a function of

binding energy at $k_\parallel$ = 0.0 Å^{-1} and hν = 22.5 eV for different photon intensities as marked.

6. Spin polarized ARPES spectra and spin angle

Figure S6 shows spin-polarized $I_{\pm\,x,y}(E)$ data. They result from the spin polarized measurements and correspond to the four spin directions S_x, $-S_x$, S_y, $-S_y$ within the surface plane of GeTe(111). Four different $\underline{k}_\parallel$-points belonging to the inner or outer surface Rashba band at E_F are selected for the analysis as displayed in the inset of Figure 4 of the main text. Notice that the finite energy resolution of the experiment provides also significant intensity above E_F. The $I_{\pm\,x,y}(E)$ data are used to determine the energy dependent spin polarization $P(E)$ displayed in Figure 4 of the main text and the energy dependent spin angle $\alpha(E)$ displayed in Figure S7 according to:

$$P(E) = \sqrt{(I_{+x} - I_{-x})^2 + (I_{+y} - I_{-y})^2}\,, \qquad \alpha(E) = \arctan\left(\frac{I_{+y} - I_{-y}}{I_{+x} - I_{-x}}\right),$$

where the sign of $I_{+y} - I_{-y}$ and $I_{+x} - I_{-x}$ is additionally considered to determine the exact angle. The resulting spin angle $\alpha(E)$ displayed in Figure S7 is almost constant for the outer bands down to -0.2 eV, while the apparent spin direction of the inner bands fluctuates with energy. The outer band i, which is probed in the region of largest separation of the two surface bands exhibits a jump by ~180° at −0.2 eV as expected for a Rashba-type band, i.e. at high energies the outer Rashba band is recorded, while at lower energies the inner Rashba band is probed at the same $\underline{k}$-point, with the latter having a spin direction rotated by 180° with respect to the former.
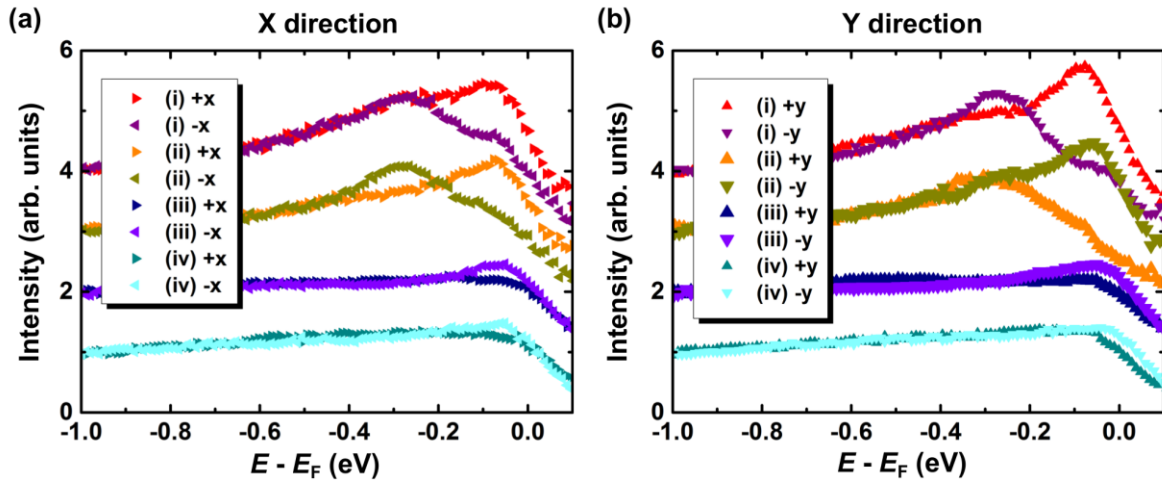
Figure S6: (a) Intensity *I* vs. electron energy *E* for spins oriented along the positive (+) and negative (-) *x*-direction, i.e. the same direction as k_x. The four $\underline{k}_{\parallel}$-points probed are labelled according to the inset in Figure 4 of the main text. (b) Same as (a) for spins oriented along the positive (+) and negative (-) *y*-direction, i.e. the same direction as k_y. Pairs of spectra are offset by one unit of the intensity scale.
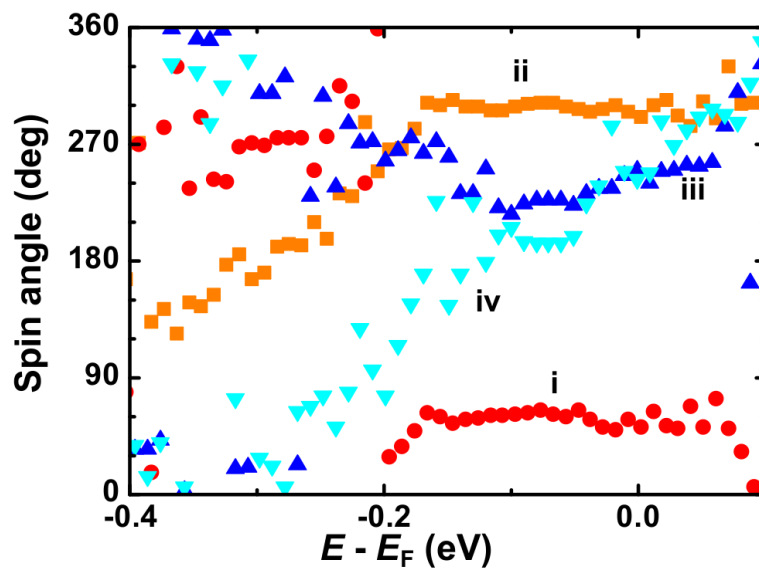

Figure S7: Deduced spin angle with respect to the horizontal axis of the inset of Fig. 4 of the main text for the $\underline{k}_{\parallel}$ values marked there.